

Ultrafast Energy Transfer Involving the Red Chlorophylls of Cyanobacterial Photosystem I Probed Through Two-Dimensional Electronic Spectroscopy

Yumin Lee¹, Michael Gorka², John H. Golbeck^{2,3} and Jessica M. Anna^{1*}

¹Department of Chemistry, University of Pennsylvania, 231 South 34 Street, Philadelphia, PA 19104, United States.

²Department of Biochemistry and Molecular Biology, The Pennsylvania State University, University Park, PA 16802, United States

³Department of Chemistry, The Pennsylvania State University, University Park, PA 16802, United States

Supporting information

List of contents

I. Details of PSI Sample Preparation.....	s2
II. Pulse Characterization: SFG-FROG.....	s3
III. Amplitude Traces for 2DES Spectra.....	s4
IV. Kinetic Model: Model 2D Spectra and Extraction of Time Constants.....	s6
V. Procedure for Extracting 2D-DAS Spectra.....	s9
VI. 2D-DAS Amplitude Traces.....	s11
VII. Singular Value Decomposition (SVD) of 2DES.....	s12
VIII. Multiple 2DES Data Sets.....	s14
IX. Power Dependence Measurements.....	s17
X. Determining the λ_1 , λ_3 Coordinates of the Equilibration Patterns.....	s21
XI. References.....	s23

I. Details of PSI Sample Preparation

Synechococcus sp. PCC 7002 and *Synechocystis sp.* PCC 6803 were grown in A+ and β -HEPES buffer, respectively. Cells were grown to an OD₇₃₀ of >2.0 in 10 L of growth media. The cells were harvested by centrifugation at 7000 x g, and lysed by three passes through a M-110EH-30 microfluidizer processor (Microfluidics). Cell debris was subsequently removed by another spin at 7000 x g. Thylakoid membranes were collected via ultracentrifugation for 1 hour at 158,000 x g and 4°C; membranes were frozen in 20% glycerol and stored at -80 °C until use. Membranes were solubilized with 1% (w/v) n-dodecyl β -D-maltoside (β -DDM) for 1 h at 4 °C in the dark and purified over a 5-20% sucrose density gradient containing 0.05% β -DDM that was spun at 28,000 rpm for 16 hours using a Beckman SW 32 Ti rotor. The trimeric band was collected and dialyzed for 4 hours against 50 mM Tris-HCl buffer (pH 8.3), and subsequently wash/concentrated over a 100 kDa amicon. The resulting solution was pelleted on a second 5-20% sucrose density gradient that lacked β -DDM. The pelleted PSI was resuspended in 50 mM Tris buffer at pH 8.3 containing 20% glycerol and 0.05% β -DDM and stored at -80 °C until use.

For the ultrafast measurements, the isolated samples were diluted with a 50 mM Tris buffer at pH 8.3 to have an OD of 0.6 at 680 nm for trimeric PSI isolated from PCC 7002 and an OD of 0.67 at 680 nm for trimeric PSI isolated from PCC 6803 in a 1 mm pathlength quartz cuvette flow cell (STARNA, 48-Q-1). 0.05% β -DDM was used as surfactant to prohibit aggregation. For the ultrafast measurements, the sample was flowed with a flow rate of 1.3 ml/min. 5 mM sodium ascorbate was added to the PSI sample to serve as a sacrificial electron donor to ensure that the ultrafast measurements were performed on open reaction centers. UV/VIS absorbance were taken before and after 2DES measurements to confirm sample integrity.

II. Pulse Characterization: SFG-FROG

The incoming laser pulses were characterized through sum frequency generation frequency resolved optical gating (SFG-FROG) with a 100 μm BBO crystal.¹ A representative projection of the cross-correlation of pump and probe pulses onto the time axis is shown in Fig. S1. According to the SFG-FROG measurements, the 2DES experiments for both PSI complexes used pulses with a FWHM of 23 fs.

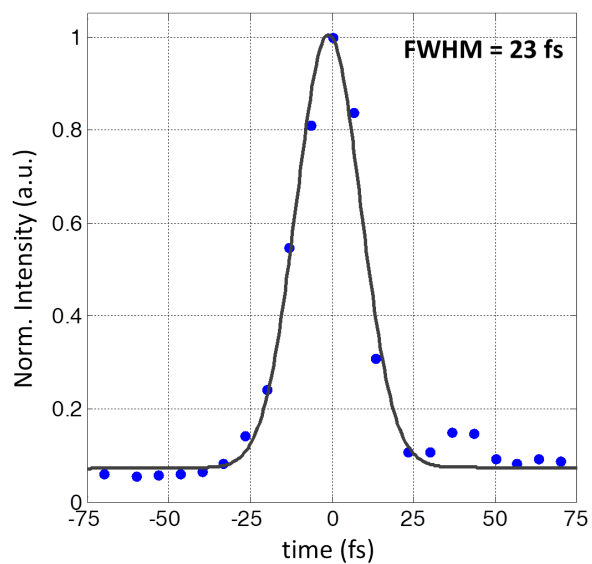


Fig. S1. Projection of the cross-correlated SFG-FROG spectra of the pump and probe pulses onto the time axis.

III. Amplitude Traces for 2DES Spectra

At different λ_1 , λ_3 coordinates the waiting time t_2 dependent amplitude of the 2DES spectra are shown in Fig. S2. The λ_1 , λ_3 coordinates are indicated in the 2DES spectra at $t_2 = 1$ ps in Fig. S2 (left) as colored dots. These coordinates and plots are the same as that of Fig. 2 in the main manuscript, but plot up to $t_2 = 300$ ps.

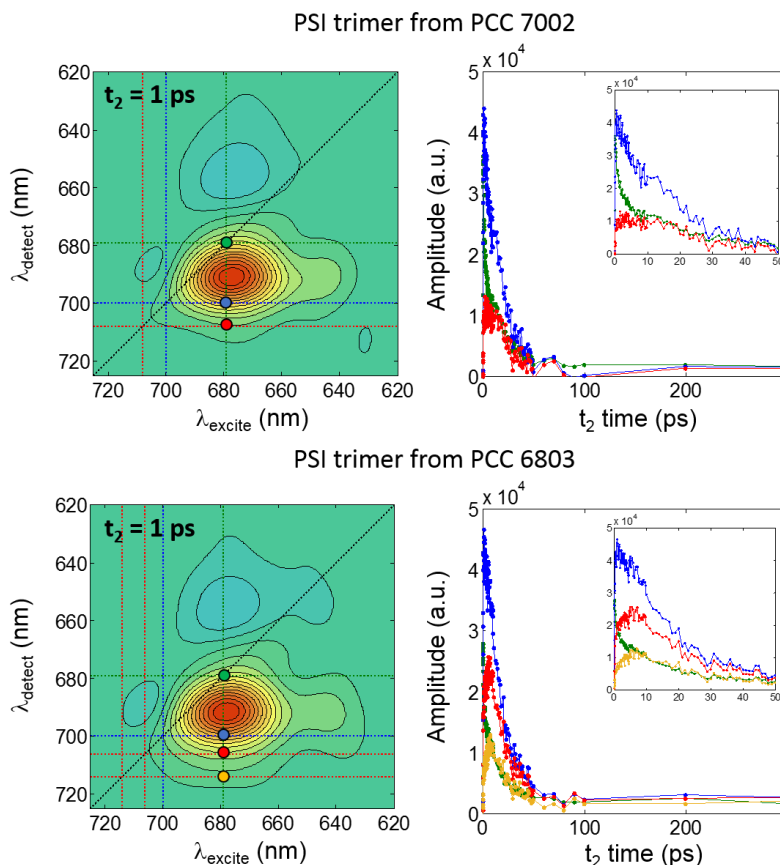


Fig. S2. Waiting time dependent amplitudes plotted up to 300 ps (right) for different λ_1 , λ_3 coordinates marked as colored dots in the 2DES spectra at $t_2 = 1$ ps (left) for PSI trimers isolated from both PCC 7002 (top) and PCC 6803 (bottom). In the left panel, zoom-in plots show the amplitude traces up to $t_2 = 50$ ps.

The traces demonstrate that the main peak corresponding to the $Q_{Y(0,0)}$ transition evolves in a complex manner. Focusing on the traces at the λ_1 , λ_3 coordinates associated with the red chlorophylls, we observe a growth followed by a decay. To compare these traces, we have applied a bi-exponential fit. The traces along with the bi-exponential fits are plotted in Fig. S3 and the rise times are reported in Table S1. Comparing the results of the bi-exponential fits demonstrates that the $Q_{Y(0,0)}$ band evolves on different timescales. From the fits, we extract a rise time of ~ 800 fs for PSI of PCC 7002. For PSI of PCC 6803, slower rise times are extracted when compared to PSI of PCC 7002, with a rise time of ~ 1 ps for red chlorophyll pool 1 and ~ 3.5 ps for red chlorophyll pool 2. Fitting results for the second red chlorophyll pool have a larger error due to the decrease in signal in this area of the 2D spectrum. According to Förster theory, the different timescales associated with the two red chlorophyll pools of PSI from PCC 6803 could arise from different spectral overlaps with different donor chlorophylls, in addition to different couplings between the red chlorophylls and the donors. However, as we are not able to discern the crosspeaks in the 2D spectra due to overlapping

spectral features, we do not focus our attention on interpreting the kinetics extracted from the traces but apply a global analysis to the data to extract different effective equilibration times for the red chlorophylls. The 2D-DAS indicate that equilibration occurs on an effective timescale of 3 ps for both pools of red chlorophylls of PSI from PCC 6803. Future work will focus on a target analysis to extract intrinsic rate constants associated with the two different pools.

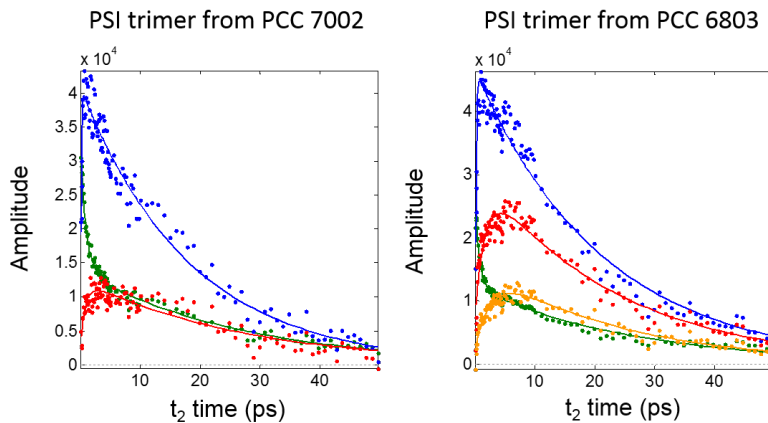


Fig. S3. The traces (dots) along with the bi-exponential fits (lines) plotted up to 50 ps for different λ_1 , λ_3 coordinates marked as colored dots in the 2DES spectra at $t_2 = 1$ ps in Fig. S2 for PSI trimers isolated from both PCC 7002 (left) and PCC 6803 (right).

Table S1. Bi-exponential fitting^a results of the traces at the λ_1 , λ_3 coordinates associated with the red chlorophylls.

		A ($\times 10^4$) ^a	B (ps) ^a	C ($\times 10^4$) ^a	D (ps) ^a
PCC7002	Red1	- 0.9 (± 0.1)	0.8 (± 0.3)	0.8 (± 0.1)	31 (± 6)
PCC6803	Red1	-1.2 (± 0.1)	1.0 (± 0.3)	1.3 (± 0.1)	35 (± 5)
	Red2	-0.8 (± 0.2)	3.5 (± 1.4)	0.8 (± 0.2)	27 (± 9)

^a Bi-exponential fitting equation is $A\exp(-t/B) + C\exp(-t/D)$, A and C are amplitudes and B and D are time constants. Reported error bars extracted from the fitting procedure represent 95 % confidence bounds.

IV. Kinetic Model: Model 2D Spectra and Extraction of Rate Constants

In order to aid in the interpretation of the 2D-DAS we introduce a model system that undergoes equilibration between two excited states. As shown in Fig. S4 our kinetic model includes two states, C_A and C_B , with transition energies having associated wavelengths ($\lambda = hc/E$) λ_A and λ_B . To model the 2D spectra and demonstrate the extracted 2D-DAS spectral patterns associated with equilibration we have allowed 2D stick spectra constructed from double sided Feynman diagrams for the model system²⁻³ to evolve according to the kinetic model shown in Fig. S4.

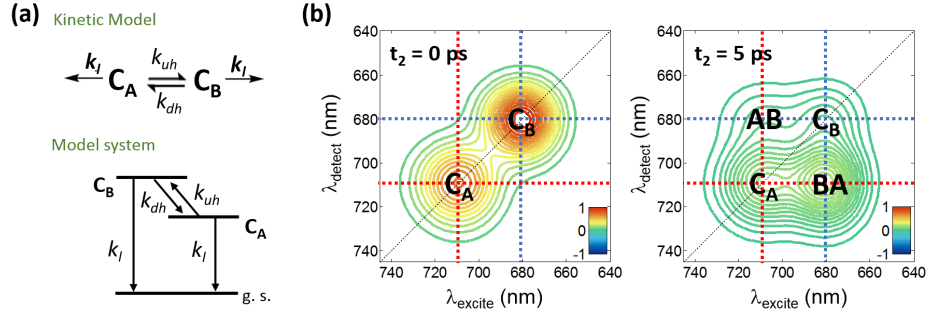


Fig. S4. (a) Schematic description of the kinetic model for equilibration between two excited state C_A and C_B . (b) 2D spectra of the model system where the dashed red lines are associated with state C_A and the dashed blue lines with state C_B . The stick spectra were described with a 2D Gaussian lineshape, and the amplitudes of the peaks were allowed to evolve according to Eq. 4.3 and 4.4.

The kinetic model and energy level diagram of the model system are shown in Fig. S4(a). The rate constant k_{dh} is the rate constant associated with the downhill energy transfer from higher frequency lying state C_B to lower lying state C_A , and rate constant k_{uh} is associated with the uphill energy transfer from C_A to C_B . The rate constants k_{dh} and k_{uh} are related through the Boltzmann factor. For the model system we have allowed both states to relax to the ground state with a rate constant k_l .

The rate equations describing the kinetic models are given by Eq 4.1 and Eq. 4.2 where N_A and N_B are the effective populations of each excited state C_A and C_B respectively.

$$\frac{dN_A}{dt} = -k_{uh}[A] + k_{dh}[B] - k_l[A] \quad \text{Eq. 4.1}$$

$$\frac{dN_B}{dt} = +k_{uh}[A] - k_{dh}[B] - k_l[B] \quad \text{Eq. 4.2}$$

The solutions to the coupled differential equation are given in Eq 4.3 and Eq 4.4, where initial conditions N_{A0} and N_{B0} were assumed to be the effective populations of state C_A ($N_A(t=0)$) and C_B ($N_B(t=0)$) immediately following excitation of the system. In the following equations, k_e , is the sum of k_{dh} and k_{uh} rate constants ($k_e = k_{dh} + k_{uh}$).

$$N_A(t) = \frac{e^{-(k_l+k_e)t} (N_{B0}(-1 + e^{k_e t})k_{dh} + N_{A0}(k_{uh} + e^{k_e t}k_{dh}))}{k_e} \quad \text{Eq. 4.3}$$

$$N_B(t) = \frac{e^{-(k_l+k_e)t} (N_{A0}(-1 + e^{k_e t})k_{uh} + N_{B0}(k_{dh} + e^{k_e t}k_{uh}))}{k_e} \quad \text{Eq. 4.4}$$

The solutions describe how the populations of C_A and C_B evolve as a function of time t . To model the 2D spectra of our model system the solutions given in Eq 4.3 and Eq 4.4 are used to weight the amplitudes of the diagonal and crosspeaks as a function of waiting time.⁴⁻⁵ Here we have chosen to represent the stick spectra as 2D Gaussians and

we note that this model does not capture lineshape evolution or molecular reorientation, but focuses on population dynamics only. Two representative 2D spectra are shown in Fig. S4(b). 2D spectra of the model system have four different peaks including diagonal peaks C_A , C_B and cross peaks BA and AB whose λ_1 , λ_3 coordinates are related to the transition frequencies ($\nu = c/\lambda$) of the two states involved in energy equilibration.

The waiting time dependence of the four different peaks is given by Eq 4.3 and Eq 4.4, where different initial conditions give the waiting time dependence of the diagonal and crosspeaks.⁴⁻⁵ The waiting time dependent amplitude of diagonal peak C_A evolves according to $N_A(t)$ (Eq. 4.3) with initial conditions set to: $N_{A0} = A_0$, and $N_{B0} = 0$. The waiting time dependent amplitude of diagonal peak C_B is given by $N_B(t)$ (Eq. 4.4) with $N_{B0} = B_0$ and $N_{A0} = 0$. For cross peak BA the waiting time dependent amplitude is given by $N_A(t)$ (Eq. 4.3) with the initial conditions set to $N_{A0} = 0$ and $N_{B0} = B_0$. In the same manner, the waiting time dependent amplitude of crosspeak AB is given by $N_B(t)$ (Eq. 4.4) with the initial conditions set to $N_{B0} = 0$ and $N_{A0} = A_0$. The expressions describing the waiting time dependence of the amplitudes for the 4 peaks in the 2D spectra are given below in Eq. 4.5 – Eq. 4.8.

$$C_A(t) = \frac{N_{A0}(k_{uh} + e^{k_e t} k_{dh})e^{-(k_l + k_e)t}}{k_e} \quad \text{Eq. 4.5}$$

$$C_B(t) = \frac{N_{B0}(k_{dh} + e^{k_e t} k_{uh})e^{-(k_l + k_e)t}}{k_e} \quad \text{Eq. 4.6}$$

$$BA(t) = \frac{N_{B0}k_{dh}(-1 + e^{k_e t})e^{-(k_l + k_e)t}}{k_e} \quad \text{Eq. 4.7}$$

$$AB(t) = \frac{N_{A0}k_{uh}(-1 + e^{k_e t})e^{-(k_l + k_e)t}}{k_e} \quad \text{Eq. 4.8}$$

2D stick spectra with 2D Gaussian lineshapes were modeled according to the above described procedure using MatLab. Representative 2D spectra for two different waiting times $t_2 = 0$ and 5 ps are shown in Fig. S4(b) with $1/k_{dh} = 3$ ps, $1/k_{uh} = 10$ ps and $1/k_l = 20$ ps and the initial peak amplitudes set to $N_{A0} = 0.7$ and $N_{B0} = 1$. k_{uh} and k_{dh} are related through the Boltzmann factor. The waiting time dependent amplitude traces for the modeled 4 peaks (Eq. 4.5 – Eq. 4.8) are plotted in Fig. S5. For a system undergoing equilibration we observe a decay of the diagonal peaks and a growth of the corresponding crosspeaks with a timescale related to $1/k_e = 1/(k_{up} + k_{dh})$.

Our 2D-DAS analysis (see section V of the supporting information) was applied to the model system to demonstrate the 2D-DAS spectral pattern associated with equilibration. Applying a global analysis we extract two different 2D-DAS components from the 2DES of the model system with associated time scales (t_n) as shown in Fig. S6. The first 2D-DAS component evolves with a time scale of 2 ps ($1/k_e = 1/(k_{up} + k_{dh})$), and the second 2D-DAS component with a time scale of 20 ps for $1/k_l$. Comparing the amplitude traces of each peak (Fig. S5) with the first 2D-DAS spectra (Fig. S6) we confirm that the positive crosspeaks in 2D-DAS indicate the growth of the corresponding crosspeaks in 2DES spectra and the negative diagonal peaks in 2D-DAS indicate a decay of the diagonal peaks on this timescale. The spectral profile of the 2D-DAS associated with equilibration is key to interpreting the 2D-DAS of the PSI complexes.

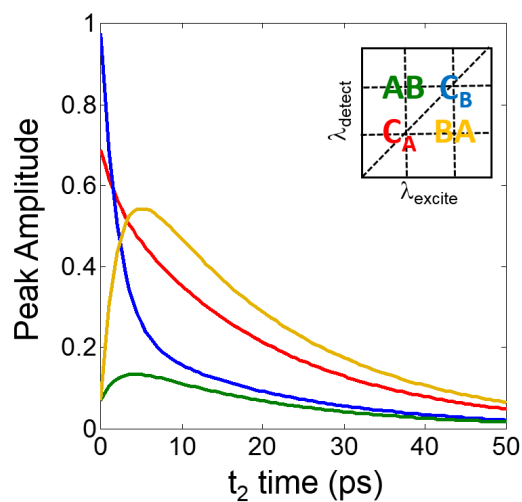


Fig. S5. Waiting time dependent amplitudes for the 4 modeled peaks where $k_{dh} = (1/3) \text{ ps}^{-1}$, $k_{uh} = (1/10) \text{ ps}^{-1}$, $k_l = (1/20) \text{ ps}^{-1}$ the initial peak amplitudes set to $N_{A0} = 0.7$ and $N_{B0} = 1$ respectively. As shown inset plot, the 4 peaks in the modeled 2DES are consistent with the diagonal peak C_A (red), diagonal peak C_B (blue), crosspeak BA (yellow), and crosspeak AB (green).

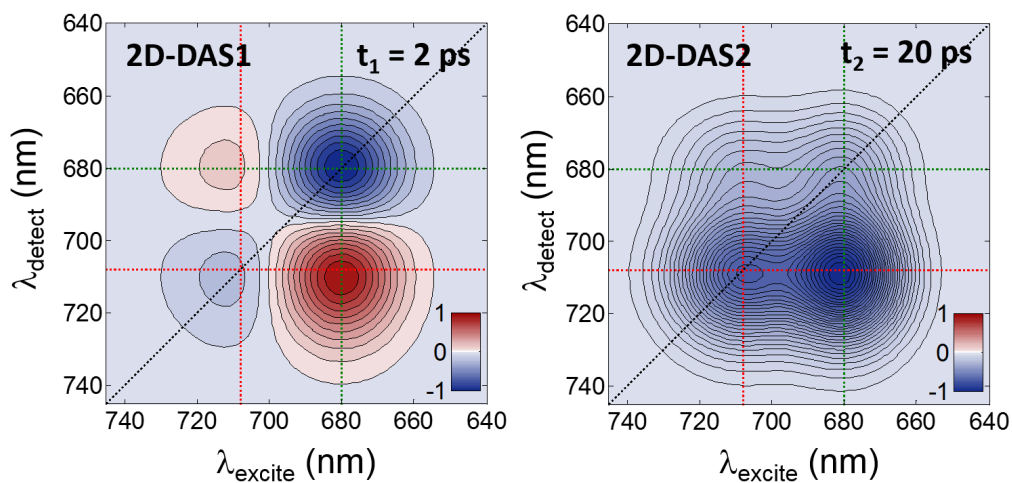


Fig. S6. Normalized 2D-DAS spectral profiles associated with the model system obtained from applying a global analysis to the 2DES spectra. The first 2D-DAS component (left) evolves with a timescale of $t_1 = 2 \text{ ps}$ and gives the characteristic spectral profile of equilibration. The second 2D-DAS component (right) evolves on a $t_2 = 20 \text{ ps}$ timescale.

V. Procedure for Extracting 2D-DAS Spectra

Global analysis is a powerful tool for unraveling multiple simultaneous kinetic processes probed with time resolved spectroscopic techniques.⁶ Applying a global analysis to the 2DES spectra of PSI, we assume that the 2DES spectra can be described as the sum of N exponential decays that have a corresponding amplitude A_n for each λ_1 , λ_3 coordinate. This is described mathematically by Eq. 5.1, where $\psi_{2DES}(\lambda_1, \lambda_3, t_2)$ is total experimental 2DES spectra and $A_n(\lambda_1, \lambda_3)$ is n^{th} 2D-DAS spectral shape among N number of distinguishable 2D-DAS components associated with the decay time constants t_n .

$$\psi_{2DES}(\lambda_1, \lambda_3, t_2) = \sum_{n=1}^N A_n(\lambda_1, \lambda_3) e^{-(t_2/t_n)} \quad \text{Eq. 5.1}$$

To extract the 2D-DAS and time constants we apply the following procedure using MatLab, which is based on previous studies.⁶⁻¹⁰ This global analysis procedure is based on the variable projection algorithm method in time resolved spectroscopy.^{6-7, 9, 11-13}

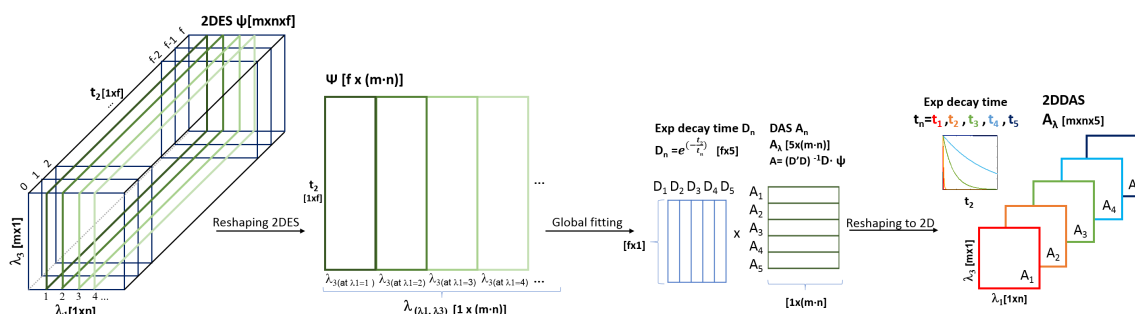


Fig. S7. Schematic description of the 2D-DAS analysis procedure. Downsampled 2DES data $\psi_{2DES}(\lambda_1, \lambda_3, t_2)$ is reshaped as the matrix $\psi_{2DES}(\lambda_{\lambda_1, \lambda_3}, t_2)$ in order to apply a global fitting procedure based on the variable projection method. Here we are considering 2DES spectra as a series of pump-probe data sets and performing a multiset analysis. The temporal components t_n are extracted from a fitting procedure and the corresponding amplitude components A_n are determined. The data is then reshaped back into the three-dimensional form yielding the 2D-DAS spectral maps.

A schematic illustrating the 2D-DAS procedure is given in Fig. S7. As shown in Fig. S7 to apply the 2D global analysis we treat the 2D data set as a multiset data structure where we consider a t_2 time-dependence of a slice along the λ_3 axis for a given λ_1 point as one data set. Here we first reshape the 2DES data from a three dimensional matrix as a function of $\lambda_1, \lambda_3, t_2$ to a 2D matrix, where a slice along the λ_3 axis for a given λ_1 is plotted as a function of t_2 . The reshaped matrix is a function of $\lambda_{(\lambda_1, \lambda_3)}$, where $\lambda_{(\lambda_1, \lambda_3)}$ has a length equal to the (length of λ_1) x (the length of λ_3). For example $\lambda_{(\lambda_1=680, \lambda_3)}$ indicates a slice along the λ_3 axis at $\lambda_1=680$ nm. The resulting reshaped 2DES spectra are given by Eq 5.2. This structure is akin to a multiset data structure, where different slices along the λ_3 axis for a given λ_1 point share the same time-dependent profile.⁸

$$\psi_{2DES}(\lambda_{(\lambda_1, \lambda_3)}, t_2) = \sum_{n=1}^N A_n(\lambda_{(\lambda_1, \lambda_3)}) e^{-(t_2/t_n)} \quad \text{Eq. 5.2}$$

Reshaping the 2DES spectra results in a 2D matrix where the columns vary as a function of wavelength and the rows vary as function of time, similar to the data organization for pump probe spectra. In this sense the reshaped 2DES data can be thought of as a multiset of pump-probe spectra for which the pump excitation frequency is varied, but where both high frequency and temporal resolution are maintained.

Equation 5.2 can be written in matrix form (Eq. 5.3) where ψ_{2DES} is a matrix with dimensions of [(m·n) x f] where m is the length of λ_1 , n is the length of λ_3 , and f is the length of the t_2 vector. A is a matrix that gives the wavelength dependent amplitudes and has dimensions of [N x (m·n)] where N is the total number of components in the system. D is a matrix describing the exponential temporal evolution ($D = e^{-(t_2/t_n)}$) and has dimensions of the [f x N].

$$\psi_{2DES} = DA^T \quad \text{Eq. 5.3}$$

In general, to extract the 2D-DAS and temporal parameters the time constants associated with the decay matrix D are estimated by minimizing the following function:

$$R = \left\| \psi_{2DES} - DA^T \right\|^2 \quad \text{Eq. 5.4}$$

To minimize Eq. 5.4 the spectral components are estimated according to the following expression, Eq. 5.5, for a given set of time constants.

$$A^T = (D'D)^{-1}D'\psi_{2DES} \quad \text{Eq. 5.5}$$

where $(D'D)^{-1}D'$ is known as Moore-Penrose pseudoinverse.^{11, 14-15} Eq. 5.4 can now be written in terms of the temporal components by substituting Eq. 5.5 into Eq. 5.4 to yield the following form for the sum of squares equation:

$$R = \left\| \psi_{2DES} - D(D'D)^{-1}D'\psi_{2DES} \right\|^2 \quad \text{Eq. 5.6}$$

The last term denotes the linear projection of ψ_{2DES} on the column space of D and the objective function is called the variable projection functional.^{11-12, 15-16} We have used the built-in lsqnonlin function in MatLab which solves non-linear least squares problems to determine the t_n parameters that globally minimize the sum of squares equation given in Eq. 5.6.¹⁶ The extracted t_n components describe how the different spectral components evolve in time. The extracted t_n components are subsequently used to determine the spectral components A_n according to Eq. 5.5. The spectral components are then reshaped into their 2D form to yield the 2D-DAS.

From our analysis we extracted 5 components (based on the 2D-SVD, see supporting information section VII). The resulting 2D-DAS for data set (*i*) are presented in the main text in Fig. 4 along with the extracted timescales, and the findings are summarized in Table 1 of the main text and Table S2 in section VIII of the supporting information. From the minimization of the sum of squares equation Eq. 5.6 we determined the values of the 5 different decay times t_n that minimized the function along with their corresponding spectral components A_n which are the 2D-DAS. The 5th component of 2D-DAS was fixed to 5 ns because it corresponds to the long-lived radical pair and does not decay on the timescale probed with our experiment. To fit the 2DES spectra we downsampled the data. Fig. S8 displays representative 2DES spectra obtained from the fitting procedure applied to data set (*i*) (See section VIII of the SI), comparing the downsampled and raw data.

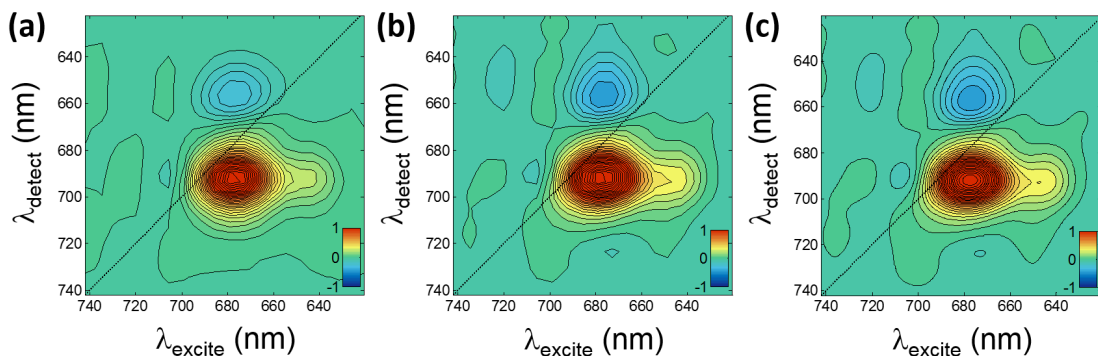


Fig. S8. Comparison of the three 2DES spectra of PSI from PCC 7002 at waiting time $t_2 = 3.7$ ps: (a) fitted 2DES spectrum (b) reduced sampling of experimental 2DES spectrum (c) experimental 2DES spectrum without downsampling

VI. 2D-DAS Amplitude Traces

From the global analysis applied to the 2DES spectra we extracted 5 different exponential time constants with corresponding 2D-DAS spectra for each PSI complex isolated from the two different cyanobacteria. The 5 extracted time constants for PSI for PCC 7002 and PCC 6803 from data set (i) are reported in Table 1 of the main text and follow here: $0.044 (\pm 0.008)$ ps, $0.200 (\pm 0.05)$ ps, $1.6 (\pm 0.3)$ ps, $19 (\pm 1)$ ps and 5 ns for PCC 7002 and $0.047 (\pm 0.006)$ ps, $0.230 (\pm 0.04)$ ps, $3.7 (\pm 0.7)$ ps, $16 (\pm 1)$ ps, and 5 ns for PCC 6803. Fig. S9 plots the normalized exponential decays associated with the 5 different 2D-DAS components for PSI complexes of PCC 7002 and PCC 6803. The color scheme of the time traces in Fig. S9 follows the same color scheme as Table 1 in the main text along with the labeling of the 2D-DAS in Fig. 4 of the main text.

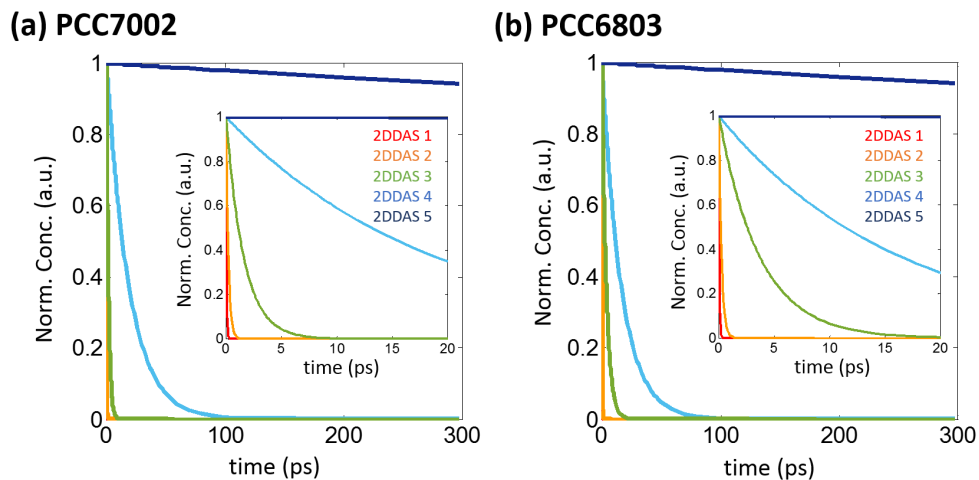


Fig. S9. 2D-DAS exponential decays (concentration traces) for the 5 different 2D-DAS components presented in Fig. 4 of the main text (color coded to be consistent with the main text) for PSI complexes of PCC 7002 (a) and for PSI complex of PCC 6803 (b) for t_2 times up to 300 ps. The insets show zoomed in plots for t_2 times up to 20 ps.

VII. Singular Value Decomposition (SVD) of 2DES

Before performing the 2D-DAS we first estimated the number of components from a singular value decomposition (SVD) performed on the 2DES spectra of PSI. For the 2D-SVD analysis the data are reshaped from a three dimensional matrix to a 2D matrix $\psi_{2DES}(\lambda_{(\lambda_1, \lambda_3)}, t_2)$ where a slice along the λ_3 axis for a given λ_1 is plotted as a function of t_2 as is described in Fig. S7. The SVD decomposition of ψ_{2DES} spectra in matrix notation is given by Eq. 7.1.^{6, 17}

$$\psi_{2DES}(\lambda_{(\lambda_1, \lambda_3)}, t_2) = U S V^T \quad \text{Eq. 7.1}$$

In Eq. 7.1, ψ_{2DES} is the reshaped 2DES matrix with dimensions of [f x (m·n)] (see section V for more details regarding reshaping). U and V are orthogonal matrices. The left matrix U has dimension of [f x f] and contains the temporal singular vectors in columns. The right matrix, V, has dimensions [(m·n) x (m·n)] and contains the spectral singular vectors in columns. S is a diagonal matrix with dimensions of [f x (m·n)] that contains the singular values along the diagonal. Applying a 2D-SVD to the PSI data we estimate the number of components $N = 5$ by the rank of ψ_{2DES} from the SVD analysis.

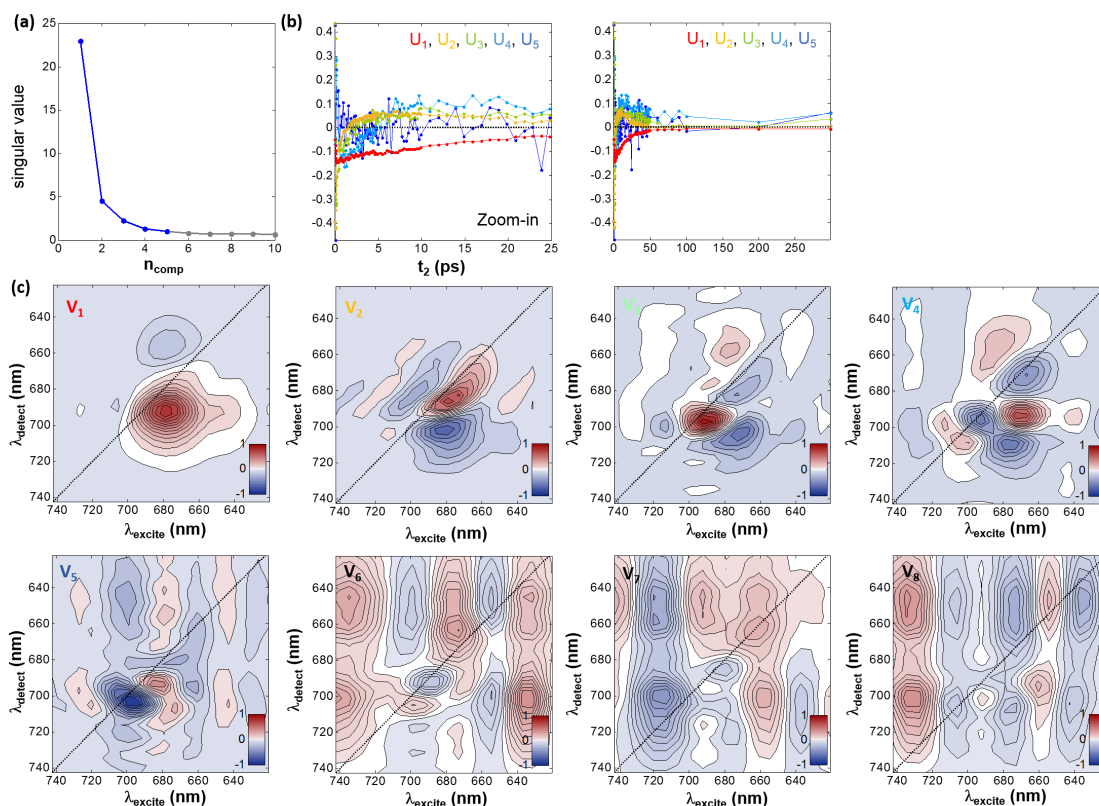


Fig. S10. 2D Singular value decomposition analysis method applied to reshaped 2DES data for PCC 6803. (a) The singular values are plotted as a function of the number of components (blue dots for components from 1 to 5 and grey dots for components from 6 to 10). (b) Plots of temporal vectors U_n ($n_{comp} = 1 \sim 5$) within waiting time $t_2 = 300$ ps (right) and zoom-in up to $t_2 = 25$ ps (left). (c) Normalized spectral vectors of V_n reshaped to 2D form for $n_{comp} = 1 \sim 8$.

Applying the SVD function in MATLAB to the reshaped 2D spectra we determined there are 5 components ($N=5$) that contribute to our spectra. As shown in Fig. S10 we determined the number of singular values to use for the 2D-

DAS analysis in terms of not only the singular values but also the shape of the spectral vector V_n in the 2D maps for each component. After the decomposition each column vector of V_n is reshaped back to the 2D spectral form $[N \times m \times n]$. In Fig. S10(c) the 8 different V_n ($N = 1\sim 8$) spectral vectors are plotted as 2D maps. The 2D maps for V_1 to V_5 show clear spectral features; however, components after V_5 lose structural shape and appear to be mostly dominated by noise. From this perspective, we could more easily determine the number of singular values needed to describe the 2DES spectra.

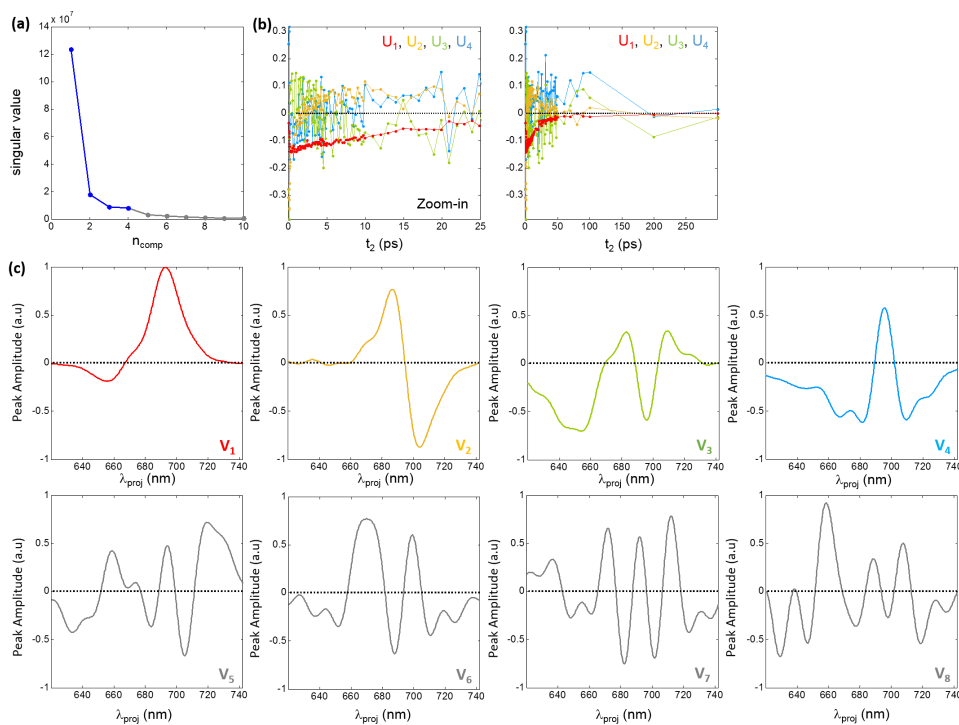


Fig. S11. Singular value decomposition analysis method applied to the projection of the 2DES onto the λ_3 axis for PCC 6803. (a) The singular values are plotted as a function of the number of components. (b) The temporal vectors U_n ($n_{\text{comp}} = 1\sim 4$) are plotted up to 300 ps (right) and up to 25 ps (left). (c) The normalized spectral vector V_n ($n_{\text{comp}} = 1\sim 8$) are plotted.

Comparing the 2D-SVD to the SVD extracted from the corresponding pump-probe spectra, we demonstrate that an additional component is extracted from the 2D-SVD.^{6, 8} For a direct comparison, we first project the 2D spectra onto the λ_3 axis (summing over λ_1) to obtain the corresponding pump-probe spectra.¹⁸⁻¹⁹ Applying a SVD to the pump-probe spectra we resolve only 4 temporal components that evolve over the timescale probed (Fig. S11). In Fig S11(c) the first 8 spectral vectors V_n are plotted. From the plots it is clear that V_1 to V_4 are distinguishable signals, where V_5 can not be distinguished from the noise.

From the comparison of the 2D-SVD and SVD, it is evident that the 2D-SVD extracts an additional component when compared to the SVD result from analysis of the corresponding pump-probe spectra. This is not surprising as the 2DES spectra can be thought of as a multiset of pump-probe spectra where each point along the 2D excitation axis can be thought of as a pump-probe spectrum taken at a different excitation frequency, but demonstrates that 2D-SVD analysis can be used to extract additional information when compared to the SVD analysis of the corresponding pump-probe spectra.

VIII. Multiple 2DES Data Sets

We collected multiple 2DES data sets for the PSI complexes isolated from different cyanobacterial species, PCC 7002 and PCC 6803 confirming that our global analysis results are reproducible. Fig. S12 and Fig. S13 display 2DES plots from three data sets referred to as (i), (ii), and (iii) for PSI complexes from PCC 7002 and PCC 6803 at three different waiting times: 40 fs, 1 ps and 20 ps. Normalized linear absorption spectra of cyanobacterial PSI complexes from PCC 7002 (green line) and PCC 6803 (blue line) along with the spectra of the incoming laser pulses (green shaded area for pump pulse and orange shaded area for probe pulse) are shown on the left side of the 2DES spectra. The 2DES data sets (i) and (ii) for PSI from PCC 7002 and PCC 6803 were taken sequentially on the same day under the same incoming pulse tuning conditions. An additional 2DES data set (iii) for PSI from PCC 6803 and PCC 7002 was taken on a different day, where slightly different spectral tunings of the incoming pump and probe pulses were employed. Though different tunings were employed we ensured that the pump and probe pulses used in all the 2DES measurements had spectral overlap with the $Q_{y(0,0)}$ transition, including the red chlorophyll pools. For each data set (i), (ii), and (iii), we applied a global analysis described in SI section V to extract the 2D-DAS spectra and time constants for each data set for each PSI complex. For all data sets the 2D-DAS spectral shapes are consistent with the 2D-DAS presented in the main manuscript and the extracted time constants and averages are reported in Table S2. Comparing the data sets demonstrates that the results are reproducible, and that the changes in spectral tuning do not greatly alter the extracted time constants (to within error) of the equilibration processes.

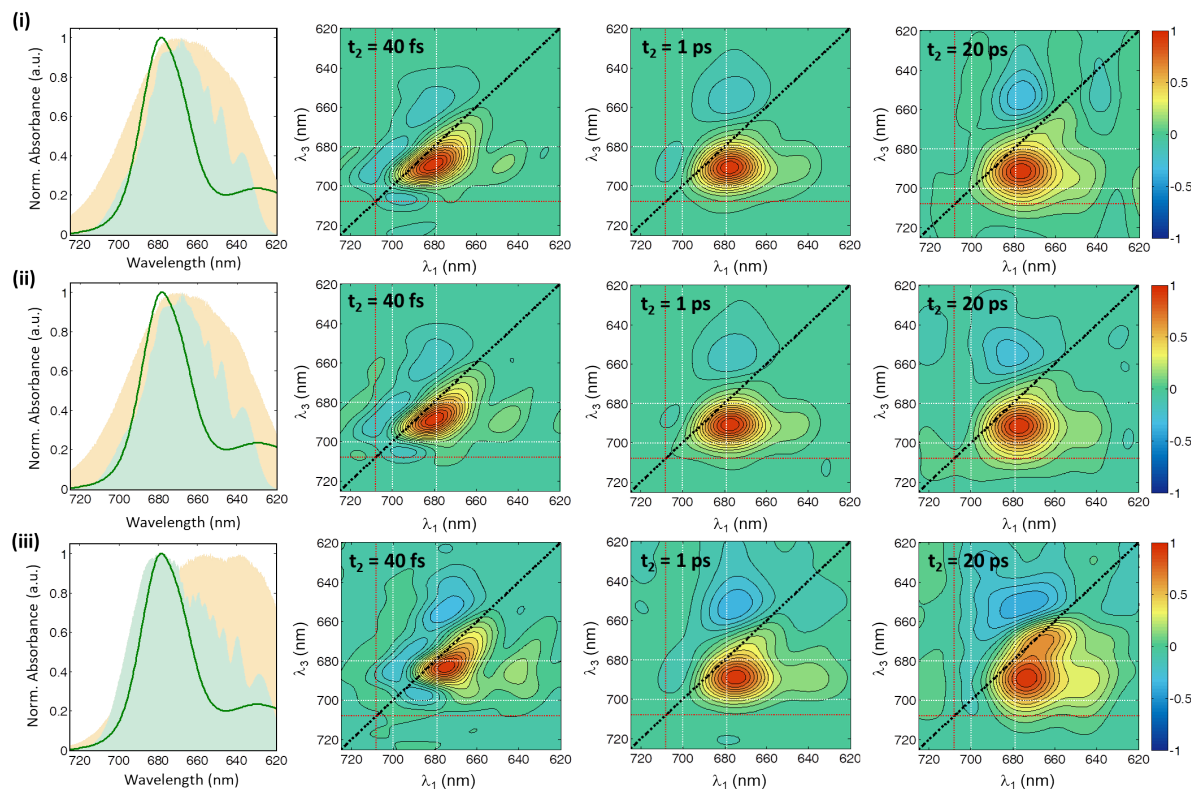


Fig. S12. Representative 2DES spectra at three different waiting time at $t_2 = 40$ fs, 1ps and 20 ps from three different data sets of PSI complexes isolated from PCC 7002 (right). On the left, normalized linear absorption spectra for PSI complexes from PCC 7002 (green line) along with the incoming pulse spectra (pump pulse – green shaded area, probe pulse – orange shaded area).

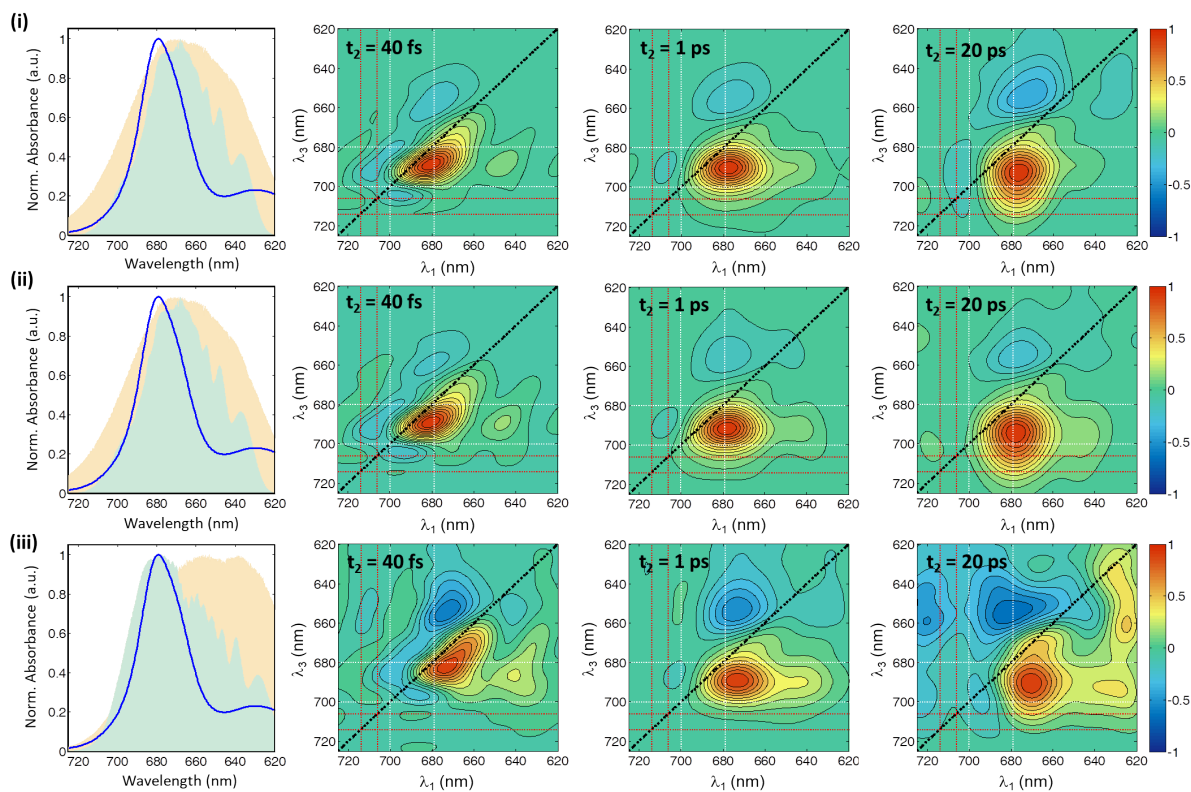


Fig. S13. Representative 2DES spectra at three different waiting time at $t_2 = 40$ fs, 1ps and 20 ps from three different data sets of PSI complexes isolated from PCC 6803 (right). On the left, normalized linear absorption spectrum for PSI complexes from PCC 6803 (blue line) are plotted along with the spectra of the incoming pulses (pump pulse – green shaded area, probe pulse – orange shaded area).

Table S2. Global analysis results of multiple 2DES data sets, (i), (ii), (iii): time constants (t_n) and maximum amplitude of 2D-DAS (A_n).

		<i>data</i>	<i>2D-DAS 1</i>	<i>2D-DAS 2</i>	<i>2D-DAS 3</i>	<i>2D-DAS 4</i>	<i>2D-DAS 5</i>
PCC 7002	t_n (ps) ^a	(i)	0.044 (± 0.008)	0.20 (± 0.05)	1.6 (± 0.3)	19 (± 1)	~ 5000
		(ii)	0.045 (± 0.014)	0.10 (± 0.03)	2.1 (± 0.5)	14 (± 1)	~ 5000
		Mean ^b	0.045 (± 0.001)	0.15 (± 0.05)	1.8 (± 0.2)	17 (± 2)	~ 5000
		(iii)	0.053 (± 0.010)	0.15 (± 0.03)	4.0 (± 0.8)	14 (± 3)	~ 5000
	A_n ^a	(i)	1.030	0.453	0.399	0.660	0.036
		(ii)	0.997	0.605	0.243	0.621	0.040
		Mean ^b	1.014 (± 0.016)	0.529 (± 0.076)	0.321 (± 0.078)	0.640 (± 0.019)	0.038 (± 0.002)
		(iii)	1.493	0.471	0.241	0.520	0.091
PCC 6803	t_n (ps) ^a	(i)	0.047 (± 0.006)	0.23 (± 0.04)	3.7 (± 0.7)	16 (± 1)	~ 5000
		(ii)	0.037 (± 0.007)	0.15 (± 0.04)	2.3 (± 0.4)	15 (± 1)	~ 5000
		Mean ^b	0.042 (± 0.005)	0.19 (± 0.01)	3.0 (± 0.7)	16 (± 1)	~ 5000
		(iii)	0.073 (± 0.015)	0.32 (± 0.09)	5.3 (± 2.0)	19 (± 6)	~ 5000
	A_n ^a	(i)	1.367	0.659	0.295	0.776	0.037
		(ii)	1.143	0.617	0.268	0.653	0.044
		Mean ^b	1.255 (± 0.112)	0.638 (± 0.021)	0.282 (± 0.013)	0.714 (± 0.061)	0.041 (± 0.003)
		(iii)	1.308	0.538	0.469	0.307	0.071
Assignment of 2D-DAS		Ultrafast relaxation	Femtosecond Energy Equilibration	Picosecond Energy Equilibration	Energy Trapping	Non-decaying P_{700^+} Component	

^a Reported error bars extracted from the fitting procedure represent one standard deviation of uncertainty for each of the data sets.

^b The reported mean value is the average of the extracted results from data sets (i) and (ii), which were obtained with the same spectral tunings. The reported mean error is the standard error (standard deviation/sqrt(number of data sets)).

IX. Power Dependence Measurements

Power dependent pump-probe and 2DES measurements were performed to determine if the extracted kinetics are dominated by annihilation effects. According to the projection slice theorem, the projection of the absorptive 2DES spectra onto the λ_3 axis is equivalent to the pump-probe spectrum taken under the same experimental conditions.¹⁸⁻¹⁹ As such, the pump-probe spectra evolve according to the same kinetics as the 2DES spectra, but require much less time to acquire compared to the 2DES measurements. For this reason we performed a systematic investigation of the power dependence using pump-probe spectroscopy, and a power-dependent 2DES measurement.

A) Power dependence pump-probe measurements

For the pump-probe measurements we varied the pump pulse power from 8 – 45 nJ, while maintaining the same pump to probe power ratio ($\text{Power}_{\text{probe}} / \text{Power}_{\text{pump}} = 0.4$). The power was adjusted using a combination of a waveplate followed by a polarizer. All of measurements were performed at the magic angle polarization. All the power dependent measurements were performed on PSI complexes isolated from PCC 6803 in a 1 mm pathlength sample cell with incoming beams focused to a spot size of $71 \mu\text{m}$ ($1/e$) at the sample position. We performed two sets of power dependent measurements with the series differing in concentration of PSI, with series 1 having an OD of 0.6 and series 2 having an OD of 0.25.

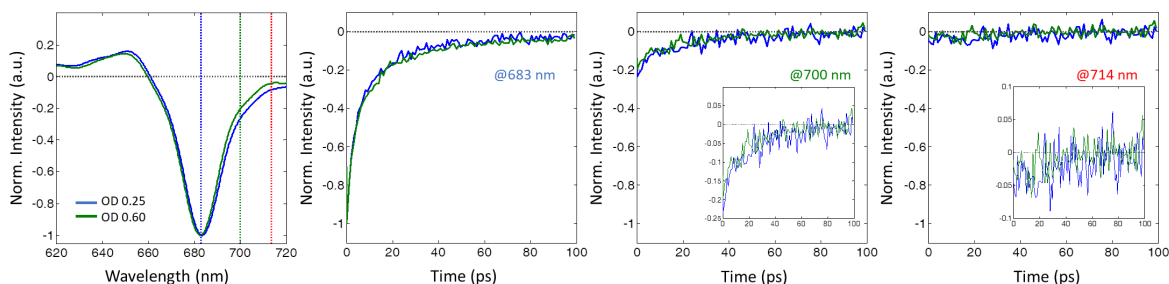


Fig. S14. Pump-probe spectra and time traces for PSI isolated in PCC 6803. In the left panel, the pump-probe spectra are plotted as a function of wavelength at waiting time $t = 10$ ps with the higher 0.6 OD concentrations shown in green and the lower 0.25 OD concentrations shown in blue. Time traces at three different wavelengths: 683 nm (blue dotted line), 700 nm (green dotted line), and at 714 nm (red dotted line) are shown with inset plots zoomed-in on the y-axis.

Fig. S14 and Fig. S15 plot the results of power dependent pump-probe measurements for the two different concentrations of PSI from PCC 6803. As shown in Fig. S14, the two series varying in OD, show similar kinetics, but the pump-probe spectra obtained with a higher OD have a better signal-to-noise ratio. To compare the kinetics, for a given pump-probe spectrum, we fit a t_2 trace taken at 680 nm with a bi-exponential function with a non-decaying component. The results of the fit are presented in Fig. S15. The results indicate that as the pump pulse power increases the error bars associated with the extracted time constants decrease – this is due to a reduction in signal to noise ratio. In addition, the results indicate that pump powers of 21 nJ (10.5 nJ/pulse in 2DES measurements) or less result in similar kinetics (to within error). For pump powers greater than 29 nJ (14.5 nJ/pulse) a decrease in the extracted time constants is observed, which is consistent with what one would expect from annihilation. The pump power employed for the 2DES experiments was ~ 21 nJ when both pump pulses are considered indicating that the presented 2D-DAS spectra and time constants are not dominated by annihilation effects.

Fig. S15 also enables a comparison between the two series differing in the OD of the sample. We find that similar kinetics are extracted for the two samples of different OD, indicating that the OD of 0.6 employed for the 2DES experiments does not lead to a change in the extracted kinetics.

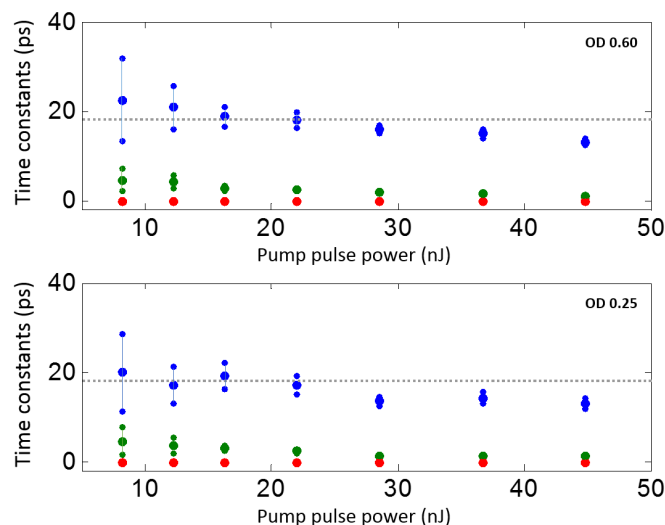


Fig. S15. The results of the bi-exponential fit with a non-decaying component are shown for traces along the t_2 axis taken at a wavelength position 683 nm (blue dotted line in Fig. S14) as a function of incoming pump pulse power. The faster exponential decay time constant is plotted in blue, the slower exponential decay time constant is plotted in green and the constant off-set is plotted in red. The top panel displays the results from pump-probe spectra obtained with higher OD of 0.6 and bottom with a lower OD of 0.25. Grey dotted lines in both plots indicate the time constants extracted from fitting the results from when the pump pulse power of 21 nJ is used, the power employed for the 2DES measurements.

B) Power dependent 2DES measurements

To further ensure that the kinetics extracted from the 2DES measurements are not dominated by annihilation effects we performed a 2DES measurement using a lower pump pulse power of 8 nJ (4 nJ per pump pulse). The 2DES spectra obtained under the different pump-power conditions are shown in Fig. S16 for PCC 7002 and Fig. S17 for PCC 6803. We note that the 2DES spectra were performed on different days with slightly different pump tunings, leading to different initial amplitudes at zero time. The t_2 dependent amplitudes for different λ_1 , λ_3 coordinates are shown in Fig. S18 for both species under different pump pulse power conditions. The λ_1 , λ_3 coordinates for the traces are indicated as colored dots on the $t_2 = 20$ ps 2DES spectra in Fig. S16 - S17. Through comparison of the traces, we confirm that the kinetics are similar, but the lower pump-power condition results in noisier 2DES data.

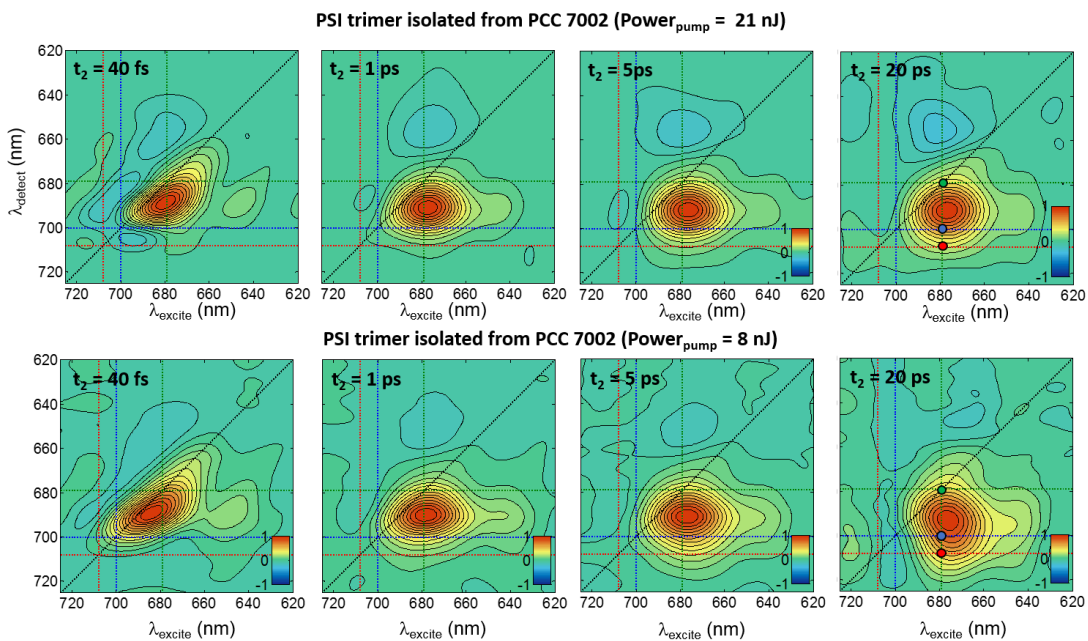


Fig. S16. 2DES spectra of trimeric PSI complexes isolated from PCC 7002 at different waiting times $t_2 = 40 \text{ fs}$, 1 ps , 5 ps , and 20 ps with 2DES data taken with an incoming pump pulse power of 21 nJ (top) and 8 nJ (bottom).

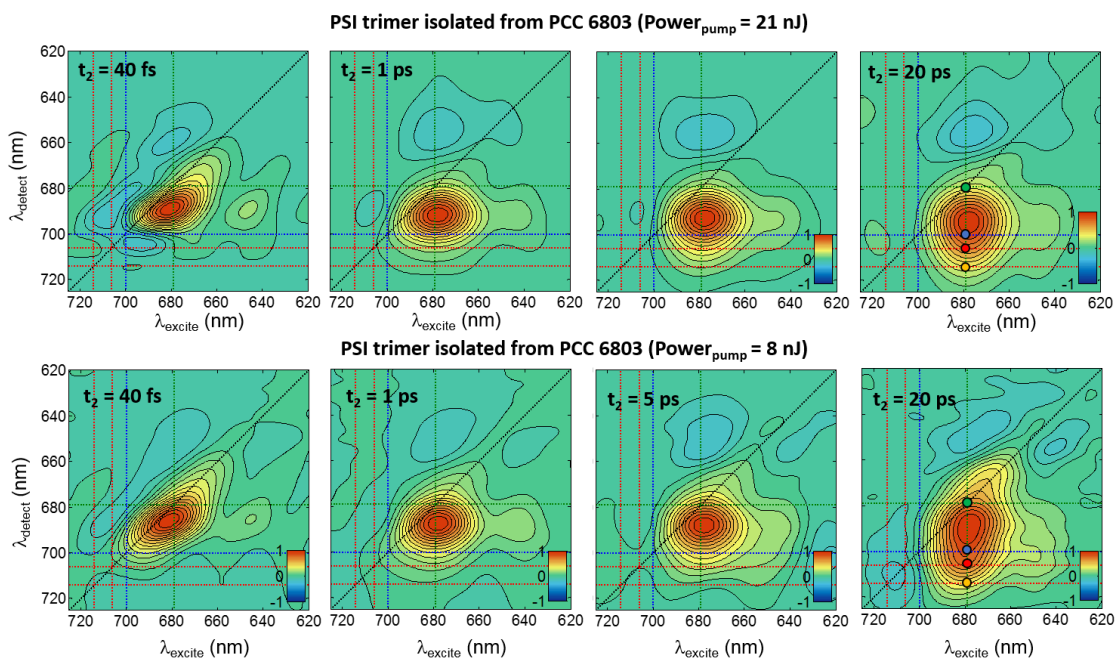


Fig. S17. 2DES spectra of trimeric PSI complexes isolated from PCC 6803 at different waiting times $t_2 = 40 \text{ fs}$, 1 ps , 5 ps , and 20 ps with 2DES data taken with an incoming pump pulse power of 21 nJ (top) and 8 nJ (bottom).

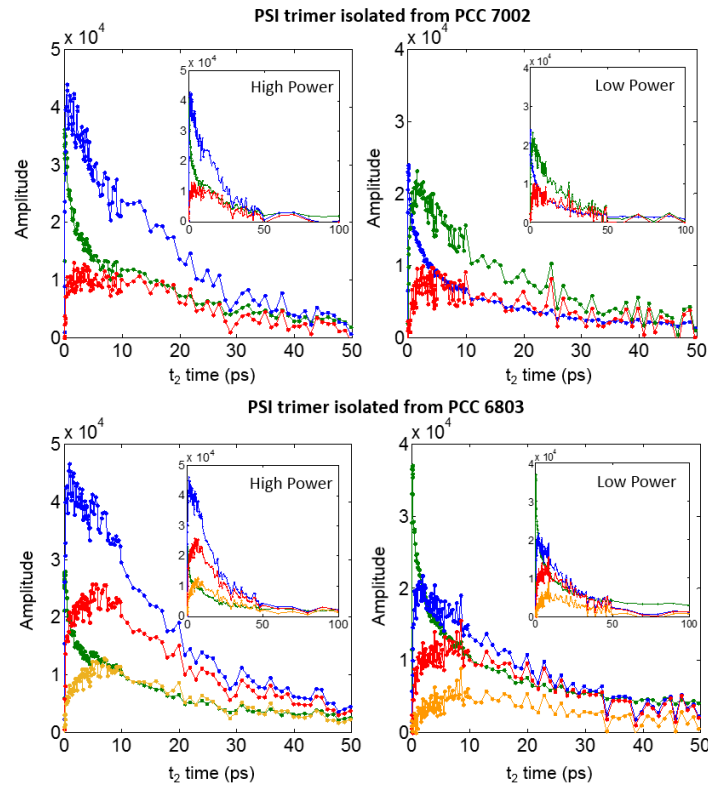


Fig. S18. Amplitudes traces for different λ_1, λ_3 coordinates (colored dots are shown in the final panel of the Fig. S16-17) as a function of the waiting time t_2 up to 50 ps and the inset shows traces for t_2 times up to 100 ps for PCC 7002 (top) and PCC 6803 (bottom). The traces from 2DES data taken under higher pump pulse powers (21 nJ) are shown on the left, and the traces from 2DES taken with lower pump pulse powers (~ 8 nJ) are shown on the right.

X. Determining the λ_1, λ_3 Coordinates of the Equilibration Patterns

The model system described in section IV demonstrates that equilibration gives a clear spectral signature in the 2D-DAS and that the λ_1, λ_3 coordinates report on the transition frequencies of the states involved in equilibration. Here we give a detailed description of our procedure for extracting the λ_1, λ_3 coordinates from the equilibration patterns observed in the 2D-DAS of PSI. The extracted λ_1, λ_3 coordinates are used to generate the boxes shown in Fig. 4 of the main text.

The λ_1, λ_3 coordinates for the boxes are determined from the two crosspeaks in the equilibration pattern. For a given crosspeak we determine the maximum amplitude of the crosspeaks and extract the λ_1, λ_3 coordinates associated with the maximum amplitude ($\lambda_{1,\max}, \lambda_{3,\max}$). In addition, we determined 95% boundary limits, indicating the point where the intensity reaches 95% of the maximum intensity. From these coordinates an inner and outer box are constructed to serve as boundary limits in interpreting the spectra. The coordinates for the inner ($\lambda_{1,\text{inner}}, \lambda_{3,\text{inner}}$) and outer box ($\lambda_{1,\text{outer}}, \lambda_{3,\text{outer}}$) are obtained from analyzing the slices along the λ_3 axis taken at $\lambda_1 = \lambda_{1,\max}$ and slices along λ_1 taken at $\lambda_3 = \lambda_{3,\max}$. For a given slice, the λ values for which the intensity decreased by 5% were determined. Where λ_- indicates the value lying to lower energies (longer wavelengths) and λ_+ indicates the value lying to higher energies (shorter wavelengths) when compared to λ_{\max} . From these values the inner and outer boxes are constructed.

Using the same peak labeling as the model system (see Fig. S4), the λ_1, λ_3 coordinates of the box are given by the following for each peak (where the subscript BA or AB refer to the two crosspeaks): BA ($\lambda_{1,\max,BA}, \lambda_{3,\max,BA}$), AB ($\lambda_{1,\max,AB}, \lambda_{3,\max,AB}$), CA ($\lambda_{1,\max,AB}, \lambda_{3,\max,BA}$), CB ($\lambda_{1,\max,BA}, \lambda_{3,\max,AB}$). The coordinates for the inner box are BA ($\lambda_{1,-,BA}, \lambda_{3,+BA}$), AB ($\lambda_{1,+AB}, \lambda_{3,-,AB}$), CA ($\lambda_{1,+AB}, \lambda_{3,+BA}$), CB ($\lambda_{1,-,BA}, \lambda_{3,-,AB}$). The coordinates for the outer box are BA ($\lambda_{1,+BA}, \lambda_{3,-,BA}$), AB ($\lambda_{1,-,AB}, \lambda_{3,+AB}$), CA ($\lambda_{1,-,AB}, \lambda_{3,-,BA}$), CB ($\lambda_{1,+BA}, \lambda_{3,+AB}$).

Using this procedure, we determined the λ_1, λ_3 coordinates for the equilibration patterns in 2D-DAS 2 and 2D-DAS 3 as shown in Fig. S19. We note for 2D-DAS 2 a clear uphill crosspeak maximum among the higher lying and lower lying state antenna states was not observed due to contributions from excited state absorption. For this equilibration pattern we assume a square box and use the coordinates of the downhill crosspeak to determine the equilibration box. The boxes are overlaid on the 2D-DAS spectra in the main text and Fig. S19 as white lines. The solid line corresponds to the box determined by the max intensity and the dashed lines correspond to the 95% limits. We note that to determine the λ_1, λ_3 coordinates we analyzed the 2D-DAS obtained from 2DES spectra that were not downsampled.

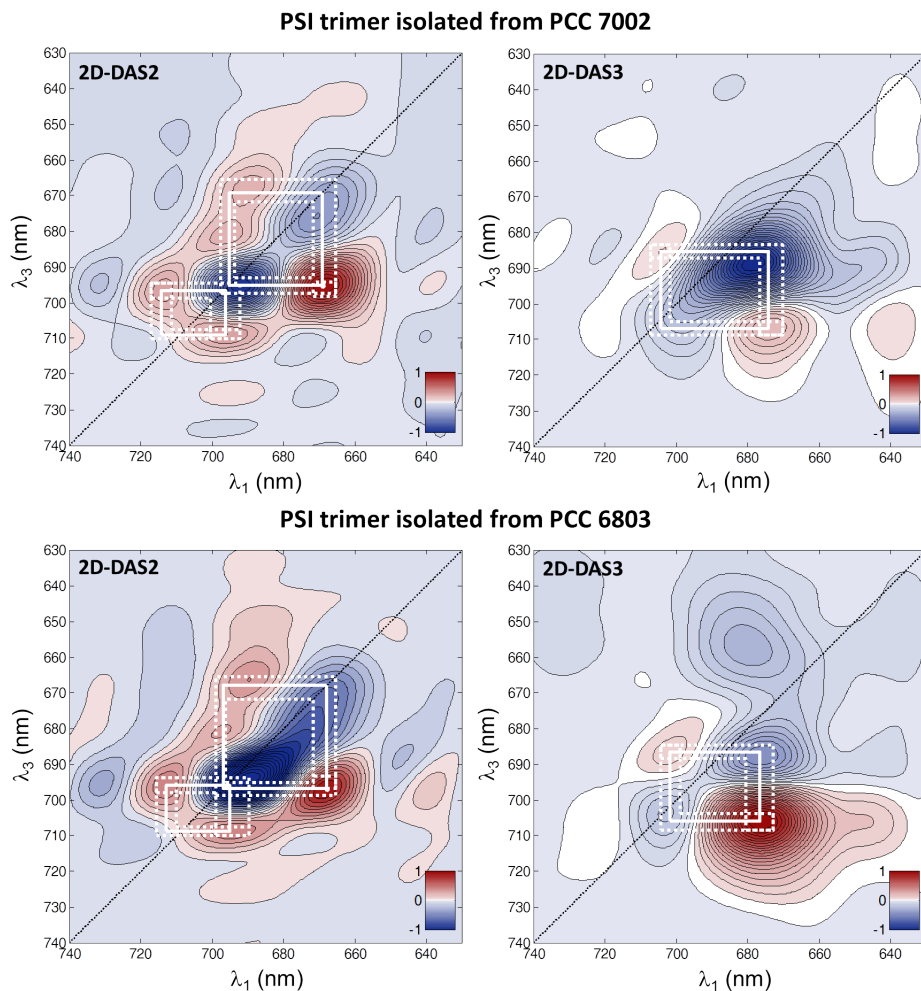


Fig. S19. 2D-DAS 2 (left) and 2D-DAS 3 (right) for PCC 7002 (top) and PCC 6803 (bottom) including the boxes (white lines) indicating the equilibration pattern among different states. Dotted white boxes indicate the inner and outer boundaries where 95% of the maximum is reached.

XI. References

- (1) DeLong, K. W.; Trebino, R.; Hunter, J.; White, W. E., *J. Opt. Soc. Am. B* **1994**, *11* (11), 2206-2215.
- (2) Mukamel, S., Principles of nonlinear optical spectroscopy. Oxford University Press: New York :, 1995.
- (3) Hamm, P.; Zanni, M., *Concepts and Methods of 2D Infrared Spectroscopy*. Cambridge University Press: New York, 2011.
- (4) Anna, J. M.; Ross, M. R.; Kubarych, K. J., *The Journal of Physical Chemistry A* **2009**, *113* (24), 6544-6547.
- (5) Kwak, K.; Zheng, J.; Cang, H.; Fayer, M. D., *The Journal of Physical Chemistry B* **2006**, *110* (40), 19998-20013.
- (6) van Stokkum, I. H. M.; Larsen, D. S.; van Grondelle, R., *Biochimica et Biophysica Acta (BBA) - Bioenergetics* **2004**, *1657* (2), 82-104.
- (7) Mullen, K. M.; van Stokkum, I. H. M., *Journal of Statistical Software; Vol 1, Issue 3 (2007)* **2007**.
- (8) Ruckebusch, C.; Sliwa, M.; Pernot, P.; de Juan, A.; Tauler, R., *Journal of Photochemistry and Photobiology C: Photochemistry Reviews* **2012**, *13* (1), 1-27.
- (9) Volpato, A.; Bolzonello, L.; Meneghin, E.; Collini, E., *Optics express* **2016**, *24* (21), 24773-24785.
- (10) Milota, F.; Prokhorenko, V. I.; Mancal, T.; von Berlepsch, H.; Bixner, O.; Kauffmann, H. F.; Hauer, J., *The Journal of Physical Chemistry A* **2013**, *117* (29), 6007-6014.
- (11) Mullen, K. M.; Vengris, M.; van Stokkum, I. H. M., *Journal of Global Optimization* **2007**, *38* (2), 201-213.
- (12) Mullen, K. M.; Stokkum, I. H. M. v., *Numerical Algorithms* **2009**, *51* (3), 319-340.
- (13) Prokhorenko, V. I., *EPA newsletter* **2012**, *June*, 21-23.
- (14) Golub, G.; Pereyra, V., *SIAM Journal on Numerical Analysis* **1973**, *10* (2), 413-432.
- (15) Gene, G.; Victor, P., *Inverse Problems* **2003**, *19* (2), R1.
- (16) O'Leary, D. P.; Rust, B. W., *Computational Optimization and Applications* **2013**, *54* (3), 579-593.
- (17) Hendler, R. W.; Shrager, R. I., *Journal of Biochemical and Biophysical Methods* **1994**, *28* (1), 1-33.
- (18) Gallagher Faeder, S. M.; Jonas, D. M., *The Journal of Physical Chemistry A* **1999**, *103* (49), 10489-10505.
- (19) Hybl, J. D.; Albrecht Ferro, A.; Jonas, D. M., *The Journal of Chemical Physics* **2001**, *115* (14), 6606-6622.